A Constitutive Model for Concrete in High Rate of Loading Conditions

Un modèle constitutif pour le béton sous sollicitations rapides

Ein Stoffmodell für Beton für grösse Beanspruchungsgeschwindigkeiten

LARSGUNNAR NILSSON
Associate Professor
Div. of Structural Engineering, University of Luleå
Luleå, Sweden

RONNY GLEMBERG
Research Associate
Dept of Structural Mechanics, Chalmers University of Technology,
Göteborg, Sweden

SUMMARY
An elastic-viscoplastic-plastic-brittle constitutive theory is chosen for concrete. It is capable of describing rate, strain history, and stress history effects, as well as the ductile and brittle failure of concrete. The model accounts for nonlinearities both in deviatoric and volumetric states of stress and strain. Comparisons with experimental results are presented.

RÉSUMÉ
Un modèle constitutif élastique-viscoplastique-plastique-fragile est choisi pour le béton. Il est capable de décrire les effets de la vitesse, de l'histoire de l'allongement, de l'histoire de la contrainte et aussi la rupture ductile et fragile de béton. Le modèle permet de tenir compte des propriétés non-linéaires dans les états de contrainte et d'allongement déviatriques et volumétriques. Des comparaisons avec des résultats expérimentaux sont présentées.

ZUSAMMENFASSUNG
Ein Stoffmodell für Beton für elastisches, viskoplastisches, plastisches und sprödes Verhalten is gewählt. Es ist möglich, Wirkungen von Geschwindigkeit, Dehnungs-Geschichte und Spannungs-Geschichte zu beschreiben. Auch spröde und duktile Brüche sind beschrieben. Das Modell kann nicht-lineare deviatorische und volumetrische Spannungs- und Dehnungs-Zustände berücksichtigen. Theoretische Ergebnisse sind mit experimentellen Resultaten verglichen.

1. INTRODUCTION

In all inelastic deformation of concrete, as well as most other materials, the response is highly dependent on the rate of stressing or straining. Furthermore, the inelastic deformation is to a large extent non-recoverable and path dependent. A realistic material model must account for these effects.

The present material model uses a combined elastic-viscoplastic-plastic-brittle theory previously presented in Nilsson [1]. This model can be motivated from the physical observations of two main stages of crack propagation: the stable crack propagation and the unstable crack propagation. Thus, the stable crack propagation will be described by the theory of viscoplasticity, and the unstable crack propagation by a combined viscoplastic-plastic, or alternatively, a combined viscoplastic-brittle theory. By the use of rate-hardening functions, the stress at failure will also depend on the strain rate.

The actual material behaviour is governed by the relative location of the stress point to the plastic yielding, brittle failure, and the viscoplastic loading surfaces in the stress space, see Figure 1.

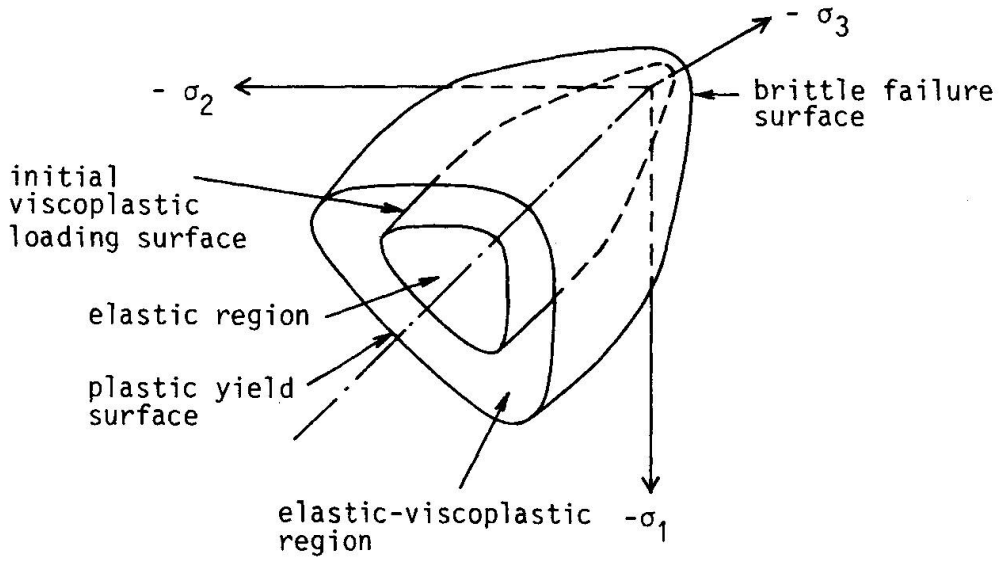

Fig 1 Regions of elasticity, viscoplasticity, plasticity, and brittle failure

2. CONSTITUTIVE EQUATIONS

2.1 Loading, potential, and failure surfaces

From proportional true triaxial tests, it is possible (within the assumption of isotropy) to construct the surface of elastic limit, the crack initiation surface, and the failure surface. Most work on the mathematical modelling of these surfaces has been concerned with the failure surface. In contrast to the failure surface, both the elastic limit surface and the crack initiation surface are closed. In the present theory, their mathematical representations are the static viscoplastic loading surface $F^V = 0$ and the plastic yield surface $F^p = 0$, respectively. For tension or combined tension-compression states of stress, the plastic yield surface is also utilized as a brittle

failure surface.

In concrete and other granular materials, strain softening and dilatancy are obtained for small hydrostatic pressures, while strain hardening and contractancy are obtained for high hydrostatic pressures. A closed loading surface and an associated flow rule are capable of modelling these effects.

A simple geometric surface, which can be made to fit the experimentally found surfaces (i.e. both $F^V = 0$ and $F^p = 0$) fairly well, is the generalized ellipsoidal surface

$$F = \left[\left(\frac{2\,\frac{\sigma_o}{H_r} - \xi_u - \xi_l}{\xi_u - \xi_l}\right)^2 + \left(\frac{\frac{\tau_o}{H_r}}{b(\theta)}\right)^2\right]^{1/2} - 1 \qquad (1)$$

where σ_o, τ_o, and θ are the octahedral normal stress, the octahedral shear stress, and the angle of similarity, respectively, given by

$$\sigma_o = \frac{1}{3}\,\mathrm{tr}\,\underset{\sim}{\sigma}, \quad \tau_o = \left(\frac{1}{3}\,\underset{\sim}{s}:\underset{\sim}{s}\right)^{1/2}, \quad \theta = \frac{1}{3}\arccos\left(\sqrt{2}\,\det(\underset{\sim}{s})/\tau_o^{\,3}\right) \qquad (2)$$

Here $\underset{\sim}{s}$ is the deviator of the stress tensor $\underset{\sim}{\sigma}$. The parameters ξ_u, ξ_l, and $b(\theta)$ can be identified from Figure 2.

The rate-hardening parameter H_r, which will later be discussed, approaches in static loading condition the value of f_{cu}.

The deviatoric semiaxis $b(\theta)$ is approximated as a function of θ (an ellipse). Due to the symmetry conditions, it suffices to interpolate b in its values b_1 and b_2 for 'triaxial extension' ($\theta = 0^o$) and 'triaxial compression' ($\theta = 60^o$)

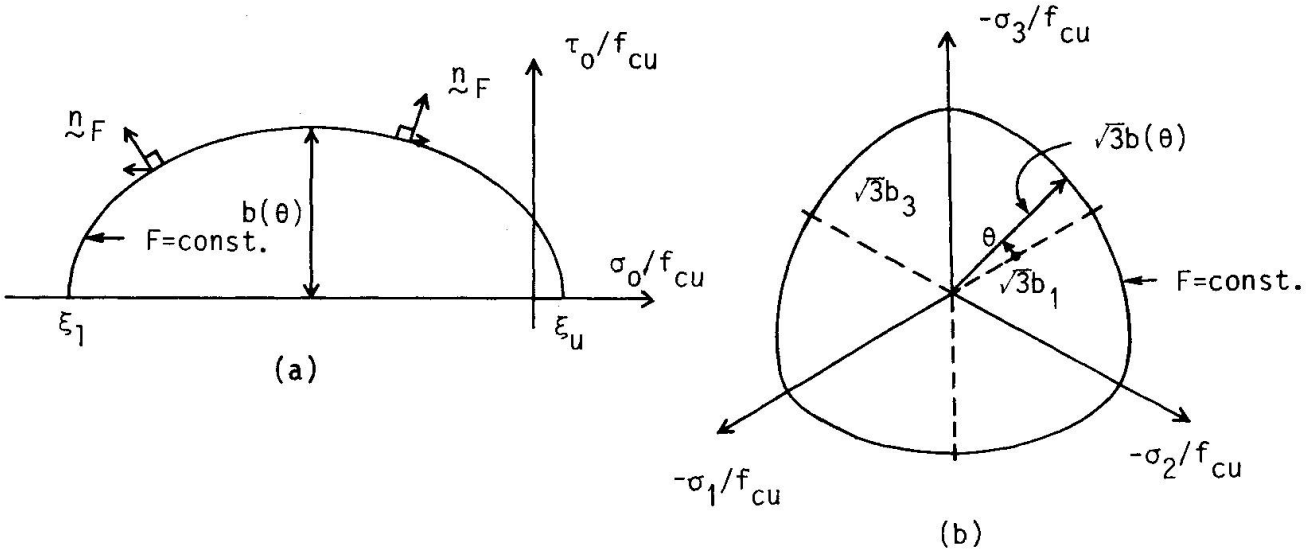

Fig 2 Rendulic (a) and deviatoric section at vertex (b) of the generalized ellipsoidal loading surface. (f_{cu} = uniaxial compressive strength)

tests, respectively. Thus,

$$b(\theta) = [t(\theta) + u(\theta)]/v(\theta) \tag{3}$$

where

$$t(\theta) = 2b_2(b_2^2 - b_1^2)\cos\theta \tag{4a}$$

$$u(\theta) = b_2(2b_1 - b_2)\,[4(b_2^2 - b_1^2)\cos^2\theta + 5b_1^2 - 4b_1b_2]^{1/2} \tag{4b}$$

$$v(\theta) = 4(b_2^2 - b_1^2)\cos^2\theta + (b_2 - 2b_1)^2 \tag{4c}$$

where $b_1 = b(0^o)$ and $b_2 = b(60^o)$, respectively, c f Figure 2(b). With the exception of the hardening and softening parameters, the generalized ellipsoidal surface contains four parameters ξ_1, ξ_1, b_1, and b_2, which must be fitted to experimental data. It is convenient to express some of these parameters in more easily identified ones, which can be obtained from standard tests: the uniaxial compressive strength f_{cu}, the uniaxial tensile strength f_{tu}, the biaxial compressive strength f_{cb}, and the elastic limit in hydrostatic compression f_{ct}. Table 1 summarizes the four different test stress states.

TABLE 1 Identification of test stress states
($\alpha_{tu} = f_{tu}/f_{cu}$, $\alpha_{cb} = f_{cb}/f_{cu}$, $\xi_1 = f_{ct}/f_{cu}$)

Test	Principal stresses	σ_o/f_{cu}	τ_o/f_{cu}	θ	$b(\theta)$
Uniaxial tension	$\sigma_1=f_{tu}$ $\sigma_2=\sigma_3=0$	$\frac{1}{3}\alpha_{tu}$	$\frac{\sqrt{2}}{3}\alpha_{tu}$	0^o	b_1
Uniaxial compression	$\sigma_1=\sigma_2=0$ $\sigma_3=-f_{cu}$	$-\frac{1}{3}$	$\frac{\sqrt{2}}{3}$	60^o	b_2
Biaxial compression	$\sigma_1=0$ $\sigma_2=\sigma_3=-f_{cb}$	$-\frac{2}{3}\alpha_{cb}$	$\frac{\sqrt{2}}{3}\alpha_{cb}$	0^o	b_1
Hydrostatic compression	$\sigma_1=\sigma_2=\sigma_3=-f_{ct}$	ξ_1	0	-	-

The following substitutions for ξ_u, b_1, and b_2 are

$$\xi_u = \frac{\alpha_{cb}^2(\frac{2}{3}\alpha_{tu} - \xi_1)^2 - \alpha_{tu}^2(\frac{4}{3}\alpha_{cb} + \xi_1)^2 - (\alpha_{cb}^2 - \alpha_{tu}^2)\xi_1^2}{2[\alpha_{cb}^2(\frac{2}{3}\alpha_{tu} - \xi_1) + \alpha_{tu}^2(\frac{4}{3}\alpha_{cu} + \xi_1) - (\alpha_{cb}^2 - \alpha_{tu}^2)\xi_1]} \tag{5}$$

$$b_1^2 = \frac{2}{9}\alpha_{cb}^2\left[1 - \left(\frac{\frac{4}{3}\alpha_{cb} + \xi_u + \xi_1}{\xi_u - \xi_1}\right)^2\right]^{-1} \tag{6}$$

$$b_2^2 = \frac{2}{9}\left[1 - \left(\frac{\frac{2}{3} + \xi_u + \xi_1}{\xi_u - \xi_1}\right)^2\right]^{-1} \tag{7}$$

For many occasions a complete set of test data is lacking, and empirical relations must be relied on. With such empirical relations, however, the number of model parameters can be reduced.

Figure 3 shows a fit of the generalized ellipsoidal surfaces to experimental data. A remarkably accurate fit for this concrete is noted for the elastic limit surface. The poorer accuracy for the fit of the initial plastic loading

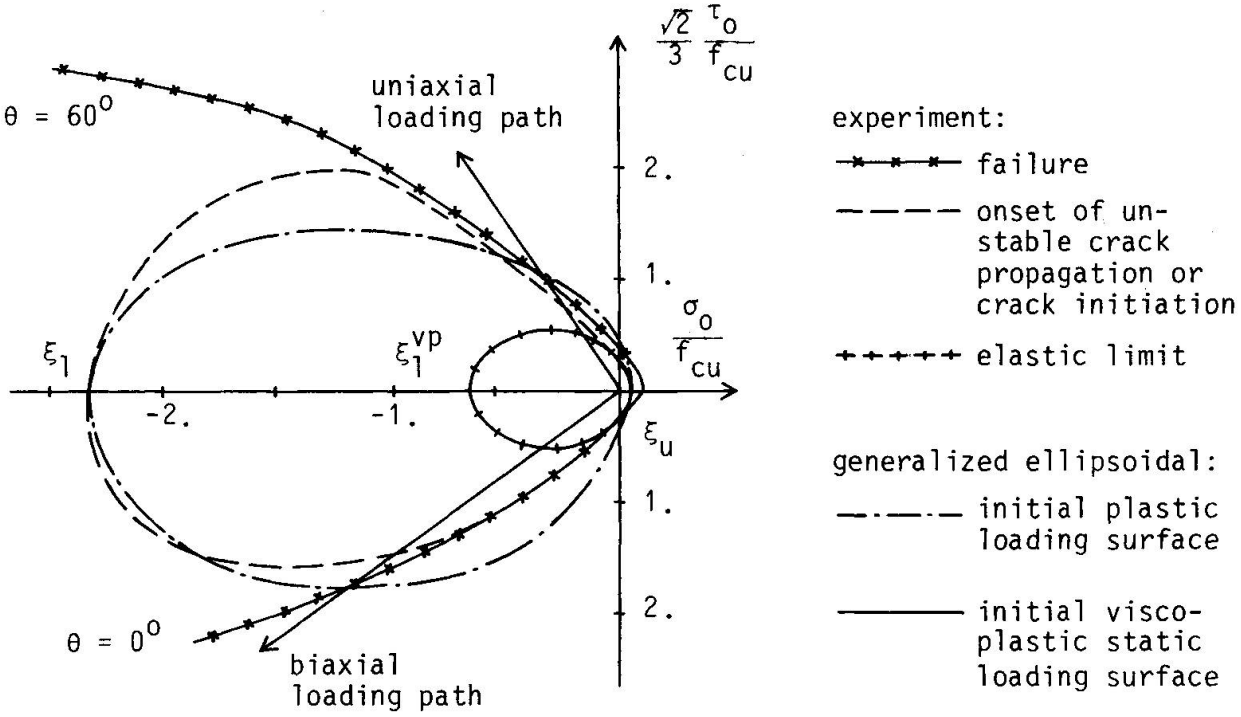

Fig 3 Fit of generalized ellipsoidal surfaces to experimental data of Launay and Gachon [2]. Parameters of the initial plastic loading surface: $\alpha_{tu} = 0.15$, $\alpha_{cb} = 1.8$, $\xi_1 = -2.3$ ($\xi_u = 0.05$, $b_1 = 0.85$, $b_2 = 0.64$). Parameters of the initial viscoplastic static loading surface: $\xi_u = 0.05$, $\xi_1 = -0.67$, $b_1 = 0.24$, $b_2 = 0.25$

surface is explained by the definite form of the ellipse. To obtain closer fits more sophisticated types of loading surfaces are needed. Another possibility for closer fits is to use two different types of loading surfaces; one of the classical type, which conforms to the failure surface, and another which intersects the hydrostatic compression axis.

2.2 Elastic response

For stress points inside the static viscoplastic loading surface, $F^v = 0$ (elastic limit surface), a hypoelastic stress-strain relation is assumed. Thus,

$$d\underset{\sim}{\sigma} = \underset{\sim}{S} : d\underset{\sim}{\varepsilon} \tag{8}$$

where $\underset{\sim}{S}$ is the fourth-order elastic tangential stiffness tensor and $d\underset{\sim}{\varepsilon}$ is the elastic strain increment tensor. Initially, a linear elastic stiffness is assumed, in which case $\underset{\sim}{S}$ contains elastic constants. For representation of stiffness degradation due to micro- and macrocracking, a dependence of the inelastic dilatance on the elastic stiffness $\underset{\sim}{S}$ is introduced in the form

$$K = {}^0K\, e^{-\left(\frac{\varepsilon_o^p}{d_1}\right)^2}, \quad G = {}^0G\, e^{-\left(\frac{\varepsilon_o^p}{d_2}\right)^2}, \quad \varepsilon_o^p > 0 \tag{9}$$

where ${}^0K$ and ${}^0G$ are the initial bulk and shear moduli, respectively, and ε_o^p is the plastic volumetric strain. The parameters d_1 and d_2 control the rate of degradation. In general we have assumed that $d_1 \equiv d_2 \equiv d$.

2.3 Elastic-viscoplastic response

For stress points in the region between the static viscoplastic loading surface, $F^v = 0$, and the plastic yield surface, $F^p = 0$, elastic-viscoplastic response is assumed. The total strain increment is additively resolved into elastic ($d\underset{\sim}{\varepsilon}^e$) and viscoplastic ($d\underset{\sim}{\varepsilon}^{vp}$) parts

$$d\underset{\sim}{\varepsilon} = d\underset{\sim}{\varepsilon}^e + d\underset{\sim}{\varepsilon}^{vp} \tag{10}$$

The elastic-viscoplastic stress-strain relation is thus

$$d\underset{\sim}{\sigma} = \underset{\sim}{S} : (d\underset{\sim}{\varepsilon} - \dot{\underset{\sim}{\varepsilon}}^{vp} dt) \tag{11}$$

The viscoplastic strain rate $\dot{\underset{\sim}{\varepsilon}}^{vp}$ is governed by a generalization of Perzyna's [3] theory

$$\dot{\underset{\sim}{\varepsilon}}^{vp} = \gamma(\dot{\underset{\sim}{\varepsilon}}, \underset{\sim}{\sigma}) < \phi(F^v) > \underset{\sim}{n}_F \tag{12}$$

where the normalized gradient $\underset{\sim}{n}_F$ of the dynamic loading potential surface, $F^v(\underset{\sim}{\sigma}, H^v) = \text{const.}$, gives the direction of the viscoplastic strain rate. The

hardening/softening function H^v will be discussed in Section 2.6. The bracket $\langle \cdot \rangle$ indicates that only values of ϕ with argument $F^v > 0$ are taken as different from zero. The static viscoplastic loading surface is given by $F^v(\underset{\sim}{\sigma}, H^v) = 0$. In short-term static and dynamic loading conditions, the primary nonlinearities of concrete are caused by microcrack growth and pore collapses. Both these physical phenomena manifest themselves as nonrecoverable delay effects. From a physical point of view, a relationship must exist between the velocity of the growth of microcracks and the viscoplastic strain rate. One can therefore interpret the accumulated viscoplastic strain as a measure of microcrack damage. Several proposals of the function $\phi(F^v)$ have been given by Perzyna [3]. They are all derived from fits to experimental data. The function

$$\phi(F^v) = \left(\frac{F^v}{F^{v1}}\right)^{\alpha} \tag{13}$$

is used in this analysis. The value F^v of the dynamic loading function is normalized against F^{v1} in order to give nondimensional values of $\phi(F^v)$. The normalization value F^{v1} has been chosen such that $F^v = F^{v1}$ at plastic yielding for a specified test state of stress. The parameter α determines the curvature of the stress-strain curve at constant rate of straining.

The parameter γ in Eq. (12) is assumed to be a function of the strain rate. This renders it possible to fit stress and strain at failure according to specified values. The following function was proposed in Nilsson [1]

$$\gamma(\dot{\varepsilon}) = \dot{\varepsilon}^{ef}\, e^{-r \ln\left|\frac{\dot{\varepsilon}^{ef}}{\dot{\varepsilon}^{ef}_r}\right|} \tag{14}$$

where $\dot{\varepsilon}^{ef}$ is an invariant function of the strain rate, $\dot{\varepsilon}^{ef}_r$ is a reference value of the effective strain rate, and r is a material constant. In the following numerical analyses

$$\dot{\varepsilon}^{ef} = (\dot{\varepsilon}_o^2 + \frac{1}{4}\dot{\gamma}_o^2)^{1/2} \tag{15}$$

has been utilized.

2.4 Elastic-viscoplastic-plastic response

For a stress point on the surface $F^p = 0$ plastic yielding takes place. The plastic strain increment $d\underset{\sim}{\varepsilon}^p$ gives a contribution to the total strain increment. Thus,

$$d\underset{\sim}{\varepsilon} = d\underset{\sim}{\varepsilon}^e + d\underset{\sim}{\varepsilon}^{vp} + d\underset{\sim}{\varepsilon}^p \tag{16}$$

It is observed that a non-zero viscoplastic strain increment always accompanies the plastic strain increment, unless the static viscoplastic loading surface at the actual stress-point coincides with the plastic yield surface.

Within the assumption of an associated flow rule the plastic strain increment is obtained from

$$d\underset{\sim}{\varepsilon}^{p} = d\lambda \frac{\partial F^{p}}{\partial \underset{\sim}{\sigma}} \tag{17}$$

where the scalar $d\lambda$ will depend on the states of stress, strain, and strain rate. During plastic flow the consistency conditions

$$F^{p}(\underset{\sim}{\sigma}, H^{p}) = 0 \qquad \text{and} \qquad dF^{p}(\underset{\sim}{\sigma}, H^{p}) = 0 \tag{18}$$

must be satisfied. If the hardening and softening of the plastic surface is governed by a function H^{p}, which is a function only of the plastic strain, we find

$$d\underset{\sim}{\sigma} = \underset{\sim}{S}^{ep} : (d\underset{\sim}{\varepsilon} - d\underset{\sim}{\varepsilon}^{vp}) \tag{19}$$

where the elastic-plastic tangential stiffness tensor $\underset{\sim}{S}^{ep}$ is given by

$$\underset{\sim}{S}^{ep} = \underset{\sim}{S} - \frac{1}{D}\left(\underset{\sim}{S} : \frac{\partial F^{p}}{\partial \underset{\sim}{\sigma}}\right)\left(\frac{\partial F^{p}}{\partial \underset{\sim}{\sigma}} : \underset{\sim}{S}\right) \tag{20a}$$

$$D = \frac{\partial F^{p}}{\partial \underset{\sim}{\sigma}} : \underset{\sim}{S} : \frac{\partial F^{p}}{\partial \underset{\sim}{\sigma}} - \frac{\partial F^{p}}{\partial H^{p}} \frac{\partial H^{p}}{\partial \underset{\sim}{\varepsilon}^{p}} : \frac{\partial F^{p}}{\partial \underset{\sim}{\sigma}} \tag{20b}$$

2.5 Elastic-viscoplastic-brittle response

Brittle failure is assumed to occur whenever the failure criterion

$$F^{c}(\underset{\sim}{\sigma}, H^{c}) = 0 \tag{21}$$

is met and at least one principal stress is positive. Before failure, isotropy is assumed, and the failure criterion (21) can be interpreted as a failure surface in the principal stress space. The shape of the failure surface changes according to the hardening and softening parameter H^{c}. The same function has been chosen both for the plastic yielding (ductile failure) and for the brittle failure. Thus, it is assumed that

$$F^{c}(\underset{\sim}{\sigma}, H^{c}) = F^{p}(\underset{\sim}{\sigma}, H^{p}) \tag{22}$$

Prior to failure the material can carry a certain amount of principal tensile stresses in any direction. Whenever the failure criterion (21) is satisfied in a spatial point, a crack plane is formed there. The crack plane induces anisotropy, which will exist for all future time. The normal of the crack plane is assumed to coincide with the direction of the maximal principal (tensile) stress at failure.

After the brittle failure, the tensile strength across the crack plane is assumed to be zero. The compressive strength across a crack plane is, however, assumed to be independent of an existing crack plane. Depending on the roughness of the crack surfaces and on the crack width (distance between the crack surfaces), the shear strength in the crack plane can vary from full strength to zero strength.

Secondary cracks may develop at a cracked point as long as a tensile strength remains in any direction. For every new crack plane that is formed, the order of the stress state will be reduced by one. Thus, prior to cracking the stress state is three-dimensional. After one crack plane has formed, it is two--dimensional, etc.

In the present analysis, the 'tension cut-off' surface is utilized as a post failure surface. Thus,

$$F^f(\underset{\sim}{\sigma}) \equiv \max\,(\sigma_i) \qquad i = 1, 2, 3 \tag{23}$$

where σ_1, σ_2, and σ_3 are the principal stresses.

At failure the following relations are satisfied:

$$F^p(\underset{\sim}{\sigma}, H_k^p) = 0 \qquad \text{and} \qquad F^f(\underset{\sim}{\sigma}) = \mu \tag{24}$$

where $\mu > 0$ is the largest principal stress. Immediately after failure, the following relation must hold

$$F^f(\underset{\sim}{\sigma} + d\underset{\sim}{\sigma}) = 0 \tag{25}$$

where $d\underset{\sim}{\sigma}$ is a stress transfer or stress relaxation. It is assumed that the incremental strain due to brittle failure $d\underset{\sim}{\varepsilon}^c$, can be added to the total incremental strain. Thus,

$$d\underset{\sim}{\varepsilon} = d\underset{\sim}{\varepsilon}^e + d\underset{\sim}{\varepsilon}^{vp} + d\underset{\sim}{\varepsilon}^c \tag{26}$$

In analogy with an associated flow theory of plasticity, it is assumed that the incremental strain due to brittle failure follows from the normality rule

$$d\underset{\sim}{\varepsilon}^c = d\lambda_c \frac{\partial F^f}{\partial \underset{\sim}{\sigma}} \tag{27}$$

where $d\lambda_c$ is dependent on the stress and strain state. Some algebra yields

$$d\underset{\sim}{\sigma} = \underset{\sim}{S}^c : (d\underset{\sim}{\varepsilon} - d\underset{\sim}{\varepsilon}^{vp}) - d\underset{\sim}{\sigma}^c \tag{28}$$

where the tangential stiffness tensor $\underset{\sim}{S}^c$ for the material with one crack plane is given by

$$\underset{\sim}{S}^c = \underset{\sim}{S} - \frac{1}{D^c}\left(\underset{\sim}{S} : \frac{\partial F^f}{\partial \underset{\sim}{\sigma}}\right)\left(\frac{\partial F^f}{\partial \underset{\sim}{\sigma}} : \underset{\sim}{S}\right) \tag{29a}$$

$$D^c = \frac{\partial F^f}{\partial \underset{\sim}{\sigma}} : \underset{\sim}{S} : \frac{\partial F^f}{\partial \underset{\sim}{\sigma}} \tag{29b}$$

and the incremental stress $d\underset{\sim}{\sigma}^c$ due to brittle failure is given by

$$d\underset{\sim}{\sigma}^c = \frac{\mu}{D^c}\ \underset{\sim}{S} : \frac{\partial F^f}{\partial \underset{\sim}{\sigma}} \tag{30}$$

The derivation of the tangential stiffness tensor $\underset{\sim}{S}^{cc}$ and the incremental fracture stress $d\underset{\sim}{\sigma}^{cc}$ due to a secondary crack plane is analogous.

Finally, when the third crack plane is formed, the tangential stiffness tensor for tensile states of stress is reduced to the zero tensor.

2.6 Strain hardening and softening

All four parameters of the generalized ellipsoidal loading surface can be functions of damage measures. This renders it possible to model complex hardening and softening behaviour. Unfortunately, much experimental results on triaxial hardening and softening of concrete are lacking, and the choice of hardening and softening functions must mainly be based on hypotheses.

Experiments show that plastic contractance hardens the material, while plastic dilatance softens the material. Thus, it is natural to use the inelastic volumetric strain as an internal variable (measure of material damage).

The parameter ξ_1 (Eq. (1)) of the generalized ellipsoidal surface is assumed to be a master hardening and softening parameter. The hardening function is obtained by identifying the inelastic strain components of experimental data obtained from hydrostatic compression tests. The exponential hardening function

$$\xi_1 = {}^0\xi_1\, e^{-a\varepsilon_o^p} \qquad (\varepsilon_o^p \leq 0) \tag{31}$$

has been found to fit test data of Green and Swanson [4] fairly well. In Eq. (31) ${}^0\xi_1$ denotes the initial hydrostatic stress at plastic yielding and a is a material parameter.

The softening function can be chosen in a similar manner from tests which exhibit softening behaviour. The following function has been chosen

$$\xi_1 = ({}^0\xi_1 + \xi_u)\, e^{-\left(\frac{\varepsilon_o^p}{b}\right)} - \xi_u \qquad (\varepsilon_o^p > 0) \tag{32}$$

where ξ_1 and ξ_u can be identified from Figure 2 and b is a material parameter. The parameter b controls the rate of softening. It has been found that $b = 5 \cdot 10^{-4}$ yields a good fit to uniaxial compression tests by Linse [5], [6]. Experimental data for the hardening and softening of the elastic limit surface seem to be lacking at present. For this reason very simple hardening and softening rules have been chosen. In the case of viscoplastic dilatancy, the relation between the parameters of the plastic yielding and the static viscoplastic loading surfaces is constant. However, plastic contractancy is assumed to affect this relation in such a way that ξ_1^{vp} tends to ξ_1. Thus

$$\xi_1^{vp} = \begin{cases} {}^0\xi_1^{vp} + \dfrac{H^v}{f_{cu}}\, \varepsilon_o^{vp} & \xi_1^{vp} > \xi_1 \\ \xi_1 & \text{otherwise} \end{cases} \tag{33a}$$

where it has been assumed that

$${}^0\xi_1^{vp} = \kappa\xi_1,\ {}^0b_1^{vp} = \kappa b_1, {}^0b_2^{vp} = \kappa b_2,\ \xi_u^{vp} = \xi_u \tag{33b}$$

and κ is a proportionality constant. The viscoplastic hardening can be explained by the observation of relatively elastic unloading paths from stress states with high hydrostatic pressure components. Furthermore, the existence of creep or relaxation even after excessive cracking can be observed in experiments.

2.7 Strain rate hardening and softening

Experiments have clearly indicated the dependence of the rate of loading or the rate of straining upon the failure. The general observation is that the ultimate stress increases significantly with the rate of loading or straining.

In the present analysis the rate effects upon the ductile yield and brittle failure surfaces are introduced in the form of a single rate hardening parameter H_r, which is a function of an effective strain rate, Eq. (15). It was proposed in Nilsson [7] that the rate hardening can be approximated as the function

$$H_r = f_{cu}\{c_1 + c_2 \ln(\dot{\varepsilon}^{ef}) + c_3[\ln(\dot{\varepsilon}^{ef})]^2\} \tag{34}$$

where the parameters c_1, c_2, and c_3 are obtained by fitting H_r to experimental data, c f Figure 4.

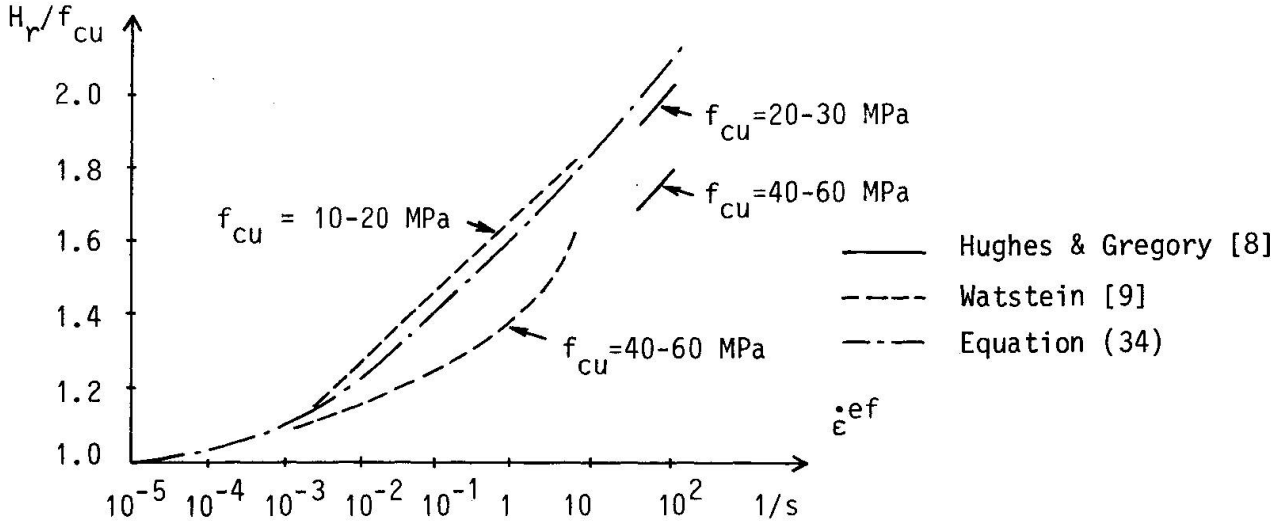

Fig 4 The effect of average strain rate upon compressive strength of concrete. Parameters of Eq. (34): $c_1 = 1.6$, $c_2 = 0.104$, and $c_3 = 0.0045$

The introduction of the hardening parameters H_r into the plastic yield and brittle failure function Eq. (1) yields an isotropic rate hardening or softening. Due to the rate effect, the failure surface can be interpreted as 'breathing'.

3. VERIFICATION OF THE CONSTITUTIVE THEORY

In this section some experimental test results found in the literature are compared to numerical results obtained with the present constitutive model. The simulations are carried out directly on the constitutive equations. Consequently, homogeneous states of stress and strain are assumed in the experimental test specimens.

In general, it is extremely difficult to perform an experimental test with all components of the strain vector prescribed according to a specified history. Most strain controlled tests have been performed with just one pre-determined strain component.

The verifications have been conducted under conditions of controlled strain rate in the smallest principal stress direction, and with a given ratio between the principal stresses. Two types of triaxial tests have been simulated: the triaxial compression test (two principal stresses equal) and the true triaxial test with constant ratio between the principal stresses.

The triaxial compression tests performed by Green and Swanson [4] were conducted on high strength concrete. According to the experimental test $f_{cu} = 48.4$ MPa and $f_{tu} = 5.6$ MPa. The biaxial strength was not tested. The following parameters have been used: $f_{cb} = 1.15$, $f_{cu} = 55.7$ MPa, $\xi_1 = -1.5$, $E_0 = 38.8$ GPa, $\nu_0 = 0.18$, $\kappa = 0.4$ (Eq. (33b)), $a = 80$ (Eq. (31)), $b = 1.0 \cdot 10^{-3}$ (Eq. (32)), $H^v = 24.0\, f_{cu}$ (Eq. (33a)), $\alpha = 0.8$ (Eq. (13)), $\dot{\varepsilon}_r^{ef} = 2.0 \cdot 10^{-6}$ s^{-1}

and $r = 0.0625$ (Eq. (14), and $d = 0.5 \cdot 10^{-3}$ (Eq. (9)). The rate of straining is assumed to be $2 \cdot 10^{-6}$ s^{-1}.

Figure 5 shows the fit of the hydrostatic compression test. With the proposed parameters the deviation between the experimental and the mathematical curves is small.

Figure 6 shows the fit of different triaxial compression tests. The hydrostatic pressure was applied in accordance with the prescribed rate of straining. When the prescribed level of lateral pressure $\sigma_1 = \sigma_2$ was reached, the lateral pressure was fixed and only the axial stress was increased according to the specified rate of straining. It is noted that relatively good fits are obtained for $\sigma_1 = \sigma_2 = 0$ and $\sigma_1 = \sigma_2 = -6.9$ MPa. Due to the lack of independent deviatoric hardening of the plastic surface, the plastic dilatance according to the model appears to be too abrupt at material instability. The disadvantage of the ellipsoidal shape of the plastic loading surface at higher hydrostatic pressures appears for $\sigma_1 = \sigma_2 = -13.8$ MPa. Furthermore, the shear compaction of the proposed model is too small.

The true triaxial tests performed by Linse [5], [6] were conducted with a constant ratio between the principal stresses. The rate of straining in the smallest principal stress direction was $2.0 \cdot 10^{-6}$ s^{-1}. The following common parameters have been used: $f_{cb} = 1.15\, f_{cu}$, $f_{tu} = 0.1\, f_{cu}$, $\xi_1 = -2.0$, $E_0 = 30.0$ GPa, $\nu_0 = 0.18$, $\kappa = 0.4$ (Eq. (33b)), $a = 100$ (Eq. (31)), $b = 0.5 \cdot 10^{-3}$ (Eq. (32)), $H^v = 50\, f_{cu}$ (Eq. (33a)), $\alpha = 0.8$ (Eq. (13)), $\dot{\varepsilon}_r^{ef} = 2.0\ 10^{-6}$ s^{-1}, $r = 0.625$ (Eq. (14)), and $d = 0.5 \cdot 10^{-3}$ (Eq. (9)).

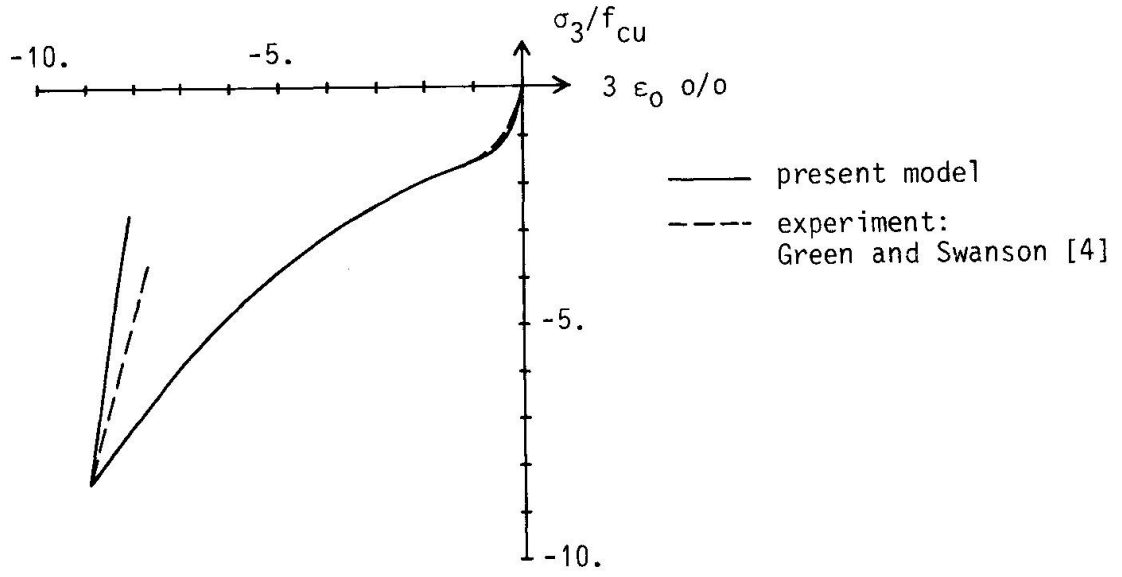

Fig 5 Fit of hydrostatic compression curve

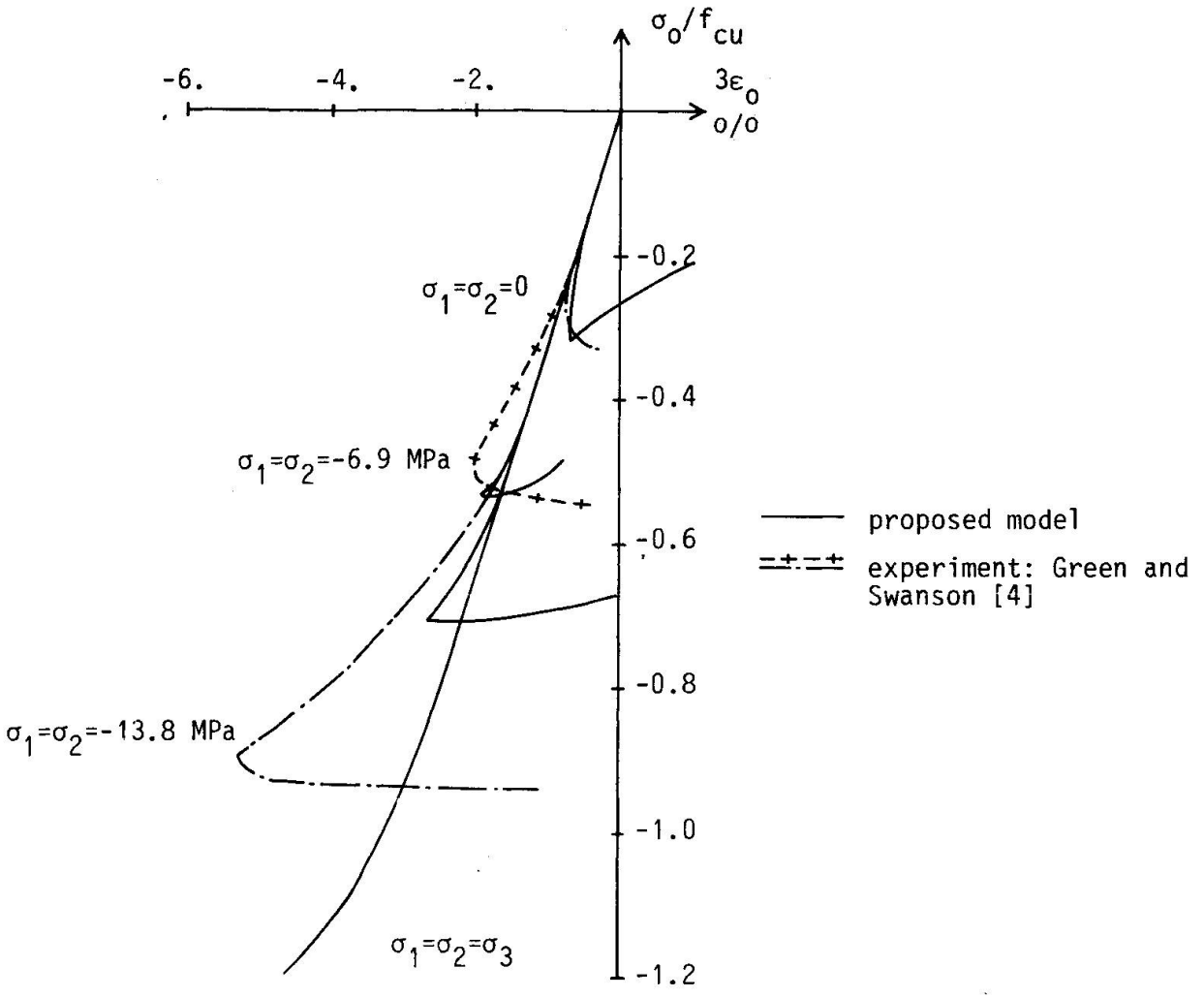

Fig 6 Fit of triaxial compression curves

Figure 7a shows the fit of a uniaxial compression curve. Some deviations between the mathematical and experimental lateral strains are observed. Figure 7b shows the corresponding fit to the biaxial loading curve. The deviations are shown to be small throughout the tested range of strains. Linse did not present any uniaxial tension test. The results from the present model, with the same material parameters as for Linse's compression tests, are shown in Figure 7c.

Figure 8a shows the performance of the present model under different loading--unloading-loading conditions conducted under constant magnitude of strain rate in the direction of maximal load (σ_3). The change of straining direction is assumed to be instantaneous. In its current version, the present model fails to describe the hysteresis loop commonly observed in cyclic tests on concrete.

Figure 8b shows uniaxial compression curves at different constant strain rates as obtained by the present model.

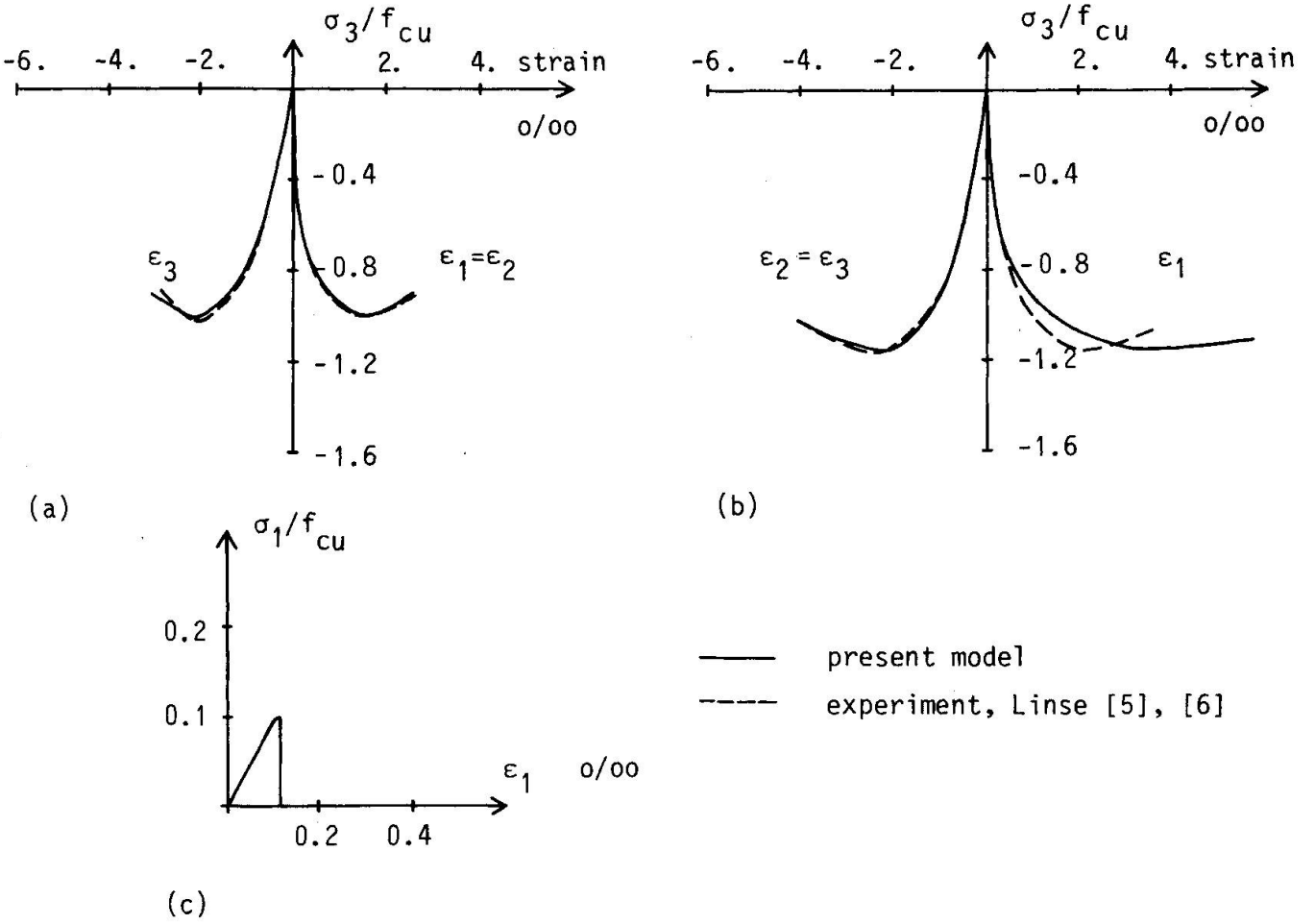

Fig 7 Uniaxial (a) and biaxial (b) compression and uniaxial tension curves (c). (f_{cu} = 30.4 MPa)

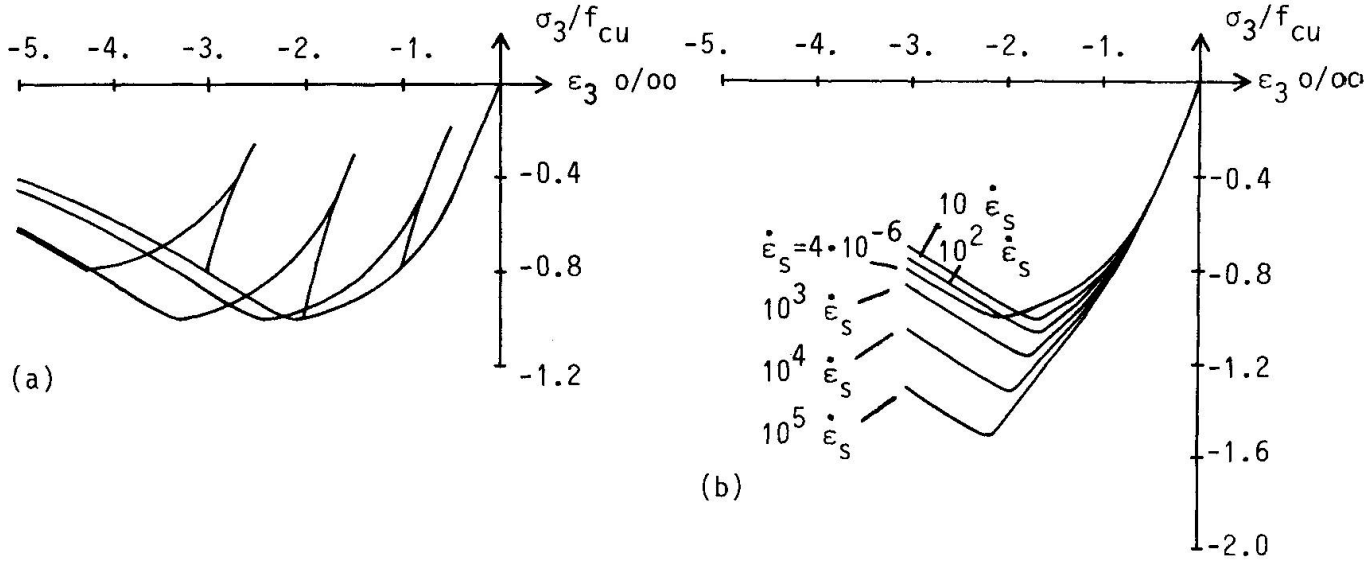

Fig 8 (a) Strain controlled cycling conducted in uniaxial compression test

(b) Uniaxial compression tests conducted at different strain rates. Constant strain rate in the direction of maximal load (f_{cu} = 30.4 MPa)

4. CONCLUDING REMARKS

The stable crack propagation and the unstable crack propagation generally observed in experiments have been modelled by the viscoplastic and plastic-brittle theories, respectively. Rate effects are included in the model both in the sense of viscoplasticity and in the form of strain rate dependent plastic loading and brittle failure relations.

From a number of verification tests, it is concluded that the present constitutive model yields results which qualitatively agree with experimental tests.

Experimental results indicate a degenerated ellipsoidal shape of the loading surface in the principal stress space. Experimental data for hardening and softening of concrete in multi-axial states of stress and strain are still not available. Thus, not much can be said about the appropriate choice of hardening and softening functions. The failure of concrete in tensile states of stress appears as a continuous softening rather than a perfect brittleness. In the present model, the directions of anisotropy of the stiffness tensor are memorized only in the case of a brittle failure. However, every kind of micro- and macro-failure of concrete introduces anisotropy into the stiffness tensor, and the directions of this anisotropy should be memorized by the material for future time.

5. REFERENCES

1. NILSSON, L.: Impact loading on concrete structures, Publication 79:1, Department of Structural Mechanics, Chalmers University of Technology, Göteborg 1979

2. LAUNAY, P. and GACHON, H.: Strain and ultimate strength of concrete under triaxial stress, Paper H1/3, Proceedings of the First International Conference on Structural Mechanics in Reactor Technology, Berlin 1971

3. PERZYNA, P.: Fundamental problems in viscoplasticity, Advances in Applied Mechanics (Eds. Chernyi et al), Vol. 9 (1966), pp 243-377

4. GREEN, S.J. and SWANSON, S.R.: Static constitutive relations for concrete, Air Force Weapons Laboratory, Technical Report No. AFWL-TR-72-2, Kirtland Air Force Base 1973

5. LINSE, D.: Versuchanlage zur Ermittlung der Dreiachsigen Festigkeit von Beton mit ersten Versuchsergebnissen, Cement and Concrete Research, Vol. 3 (1973), No. 4, pp 445-457

6. LINSE, D.: Lösung versuchstechnischer Fragen bei der Ermittlung des Festigkeits- und Verformungsverhaltens von Beton unter dreiachsiger Belastung, Deutscher Ausschuss für Stahlbeton, Heft 292, 1978

7. NILSSON, L.: Finite element analysis of impact on concrete structures, Finite Elements in Nonlinear Mechanics (Eds. Bergan, P. et al), Tapir, Trondheim 1978

8. HUGHES, B.P. and GREGORY, R.: Concrete subjected to high rates of loading in compression, Magazine of Concrete Research, Vol. 24 (1972), No. 78, pp 25-36

9. WATSTEIN, D.: Properties of concrete at high rates of loading, Symposium on Impact Testing, ASTM, STP 176, 1976, pp 156-169